J. Fluid Mech. (2012), *vol.* 700, *pp.* 382–405.
doi:10.1017/jfm.2012.138

Development of the trailing shear layer in a starting jet during pinch-off

L. Gao† and S. C. M. Yu

Division of Aerospace Engineering, School of Mechanical and Aerospace Engineering, Nanyang Technological University, Singapore 639798, Singapore

(Received 23 April 2011; revised 13 February 2012; accepted 7 March 2012; first published online 30 April 2012)

Experiments on a circular starting jet generated by a piston–cylinder arrangement, over a range of Reynolds number from 2600 to 5600, are conducted so as to investigate the development of the trailing shear layer during the leading vortex ring formation, as well as the corresponding effects on the pinch-off process. Results obtained by digital particle image velocimetry (DPIV) show that secondary vortices start to develop in the trailing jet only after the critical time scale, the 'formation number', is achieved. The subsequent growth of the secondary vortices reduces the vorticity flux being fed into the leading vortex ring and, as a consequence, constrains the growth of leading vortex ring with larger circulation. Evolution of perturbation waves into secondary vortices is found to associate with growth and translation of the leading vortex ring during the formation process. A dimensionless parameter 'A', defined as $\Gamma_{ring}/(x_{core}\Delta U)$, is therefore proposed to characterize the effect of the leading vortex ring on suppressing the nonlinear development of instability in the trailing shear layer, i.e. the initial roll-up of the secondary vortices. In a starting jet, A follows a decreasing trend with the formation time t^*. A critical value $A_c = 1.1 \pm 0.1$ is identified experimentally, which physically coincides with the initiation of the first secondary vortex roll-up and, therefore, indicates the onset of pinch-off process.

Key words: shear layers, vortex dynamics

1. Introduction

In general, a starting jet is referred to as the initial development of a jet in which a column of fluid is issued from a nozzle or an orifice into the quiescent environment. The dynamics of the leading vortex ring, which is formed by the roll-up of the separated cylindrical shear layer from the edge of the nozzle or orifice exit (Didden 1979), actually determine the characteristics of the starting jet, such as jet penetration, ambient fluid entrainment and thrust generation. One of the most important features about the leading vortex ring formation is its disconnection from the generating jet at a critical dimensionless time t^* ($t^* = \bar{U}_p t/D$, where $\bar{U}_p$ is the running average of the piston velocity and D is the nozzle diameter), because it imposes an upper limit to the growth of the leading vortex ring. This phenomenon was first observed experimentally and termed as 'vortex ring pinch-off' by Gharib, Rambod & Shariff (1998). They defined the critical value of the formation time as the 'formation number' F, and

† Email address for correspondence: LGAO@ntu.edu.sg

found that its value was in the range of 3.6–4.5 for a variety of jet exit geometries, Reynolds numbers and velocity programs. Although the formation number is a relatively universal value for starting jets generated by the piston–cylinder arrangement, subsequent investigations found that it may vary by some other parameters of the staring jet, such as velocity profiles at the nozzle exit (Rosenfeld, Rambod & Gharib 1998; Mohseni, Ran & Colonius 2001), external background flow (Dabiri & Gharib 2004; Krueger, Dabiri & Gharib 2006) and temporal-varying exit diameter (Allen & Naitoh 2005; Dabiri & Gharib 2005). As a consequence, the final state of the leading vortex ring, such as its dimensionless energy and circulation, also varies among different starting jet configurations.

Two theoretical explanations have been proposed for the vortex ring pinch-off observed in starting jets with the piston–cylinder arrangement. Existence of the critical dimensionless time scale in vortex ring formation was first discussed by Gharib *et al.* (1998) in terms of the Kelvin–Benjamin variational principle (Kelvin 1880; Benjamin 1976), which states that a steadily translating vortex ring has maximum energy with respect to the equivalent rearrangements of its vorticity that maintain the same total impulse. Accordingly, a forming vortex ring can only accept additional vorticity and subsequently relax to a new configuration if the impulse-normalized energy of the new configuration is greater than that of an alternative vortex ring/shear layer configuration in which the additional vorticity is not accepted by the vortex ring. Therefore, the pinch-off process can be considered as a relaxation process of the leading vortex ring to an equilibrium state. In addition to the relaxation explanation, Mohseni *et al.* (2001) explained the pinch-off process in terms of the translational dynamics of the leading vortex ring and its trailing jet. Based on the fact that the growth of the leading vortex ring is supported by the trailing shear layer, they suggested a kinematic explanation that the pinch-off occurs when the translational velocity of the leading vortex ring becomes equal to the local axial velocity of the trailing jet, i.e. the time when the leading vortex ring starts to translate faster than the trailing jet. Based on the above two theoretical explanations, several analytical models (Mohseni & Gharib 1998; Shusser & Gharib 2000; Gao & Yu 2010) have been developed to predict the existence of the limiting time scale for the vortex ring formation in a starting jet.

These explanations, however, ignore a fundamental feature of the starting jet, i.e. the development of instability in the trailing shear layer. For a starting jet with large stroke ratio L/D, it is observed that secondary vortices (or equally termed as trailing vortices relative to the leading vortex ring) could be formed in the trailing shear layer. Zhao, Frankel & Mongeau (2000) found by numerical simulation that the Kelvin–Helmholtz-type vortices formed in the trailing jet would absorb vorticity being fed into the leading vortex ring. Since the growth of the leading vortex ring is sustained by the influx of mass, vorticity, momentum and kinetic energy from its trailing shear layer at a specific rate, the development of trailing jet instability would play a fundamental role in the vortex ring pinch-off process. A better understanding of the effect of trailing jet instability in a starting jet might offer a new perspective to explain the underlying physical mechanism which constrains the growth of the leading vortex ring in a starting jet.

The studies on the role of the development of the trailing shear layer in a starting jet are still limited. By examining the effects of Reynolds number and shear layer thickness, Zhao *et al.* (2000) found that approximately 20 % variation of the formation number and vortex ring circulation at different values of Reynolds number and boundary layer thickness δ^* should be attributed to the trailing jet instability. The trailing shear layer is more unstable and susceptible to Kelvin–Helmholtz instability

Case	Maximum piston velocity U_{max} (m s^{-1})	Reynolds number Re_D
C1	0.222	5600
C2	0.160	4100
C3	0.101	2600

TABLE 1. Summary of experimental parameters.

at higher values of Re and smaller values of δ^*. Nevertheless, the development of the trailing jet instability and the dynamics of secondary vortices during the initial vortex ring formation and pinch-off process have not been investigated in previous literature.

The present study is intended to elaborate on the effects of trailing jet instability on the pinch-off process via experiments and theoretical analysis. The experimental set-up and procedures are briefly described in § 2. This is followed by the discussion on the development of secondary vortices (i.e. large coherent structures) in the trailing jet, as well as its effect on the growth of the leading vortex ring in § 3. The characteristics of the trailing jet instability during the initial vortex ring formation and pinch-off process are presented and explained in § 4, by considering the influence of the leading vortex ring. Based on experimental results on the trailing jet development, an alternative explanation for the pinch-off process is proposed and the physical meaning of the formation number is interpreted in terms of a new dimensionless parameter in § 5. The paper ends with brief concluding remarks.

2. Experimental set-up

The experimental set-up is shown schematically in figure 1. Experiments are conducted in a plexiglas tank with dimensions of 0.5 m × 0.6 m × 1.3 m, which is filled with tap water and kept at room temperature (20 °C). The starting jet is generated horizontally by a piston–cylinder mechanism. The cylindrical nozzle has an inner diameter of $D = 2.54$ cm. The outer wall of the nozzle near the exit is shaped to form a wedge with a tip angle of 20° so as to diminish the influence of the exit lip thickness on the circulation of the leading vortex ring. The length of the nozzle is 36 cm and the maximum stroke length of the starting jet in this experiment can reach $L_{max} = 36$ cm/2.54 cm $\approx 14D$, which is sufficiently long to observe the entire formation and pinch-off process of the leading vortex ring. The velocity history of the piston is controlled by a solenoid valve (Burkert 6024 in combination with Burkert 8623-2 PI controller) and monitored by an ultrasonic flowmeter (Shenitech STUF-200F1G), which is connected to a PC via a data acquisition card (NI USB-6251).

A total of 43 runs with different velocity programs and Reynolds numbers have been conducted, but only results from the three most representative piston velocity programs, as shown in figure 2, will be discussed in detail in the following sections. Following Rosenfeld *et al.* (1998) and Krueger & Gharib (2003), the Reynolds number for these non-impulsively started velocity programs is defined as

$$Re_D = \frac{U_{max} D}{\nu}, \tag{2.1}$$

where U_{max} is the maximum $U_p(t)$ achieved during jet ejection. The main flow conditions are summarized in table 1.

The flow field measurements of the starting jet are obtained by using digital particle image velocimetry (DPIV). Polyamide seeding particles (PSPs) manufactured

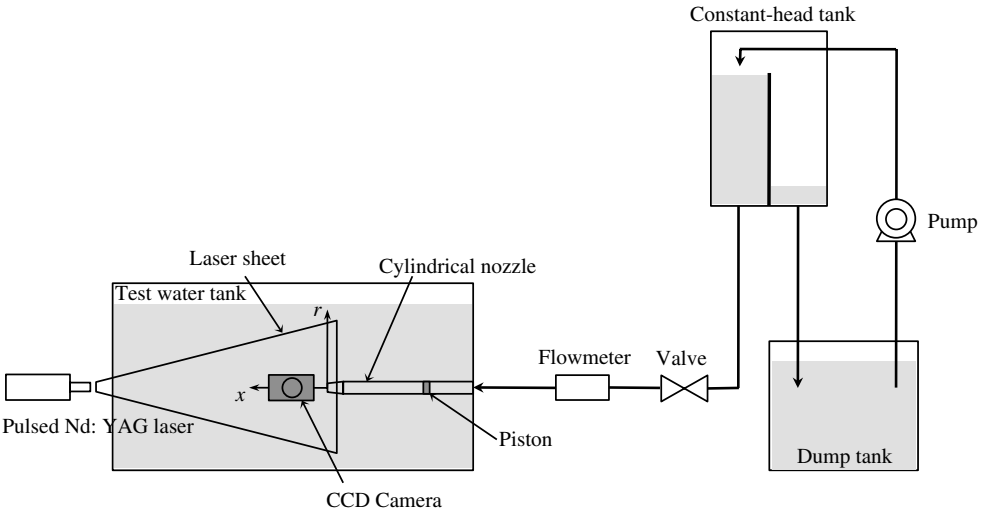

FIGURE 1. Schematic of the experimental apparatus for starting jet generation with a piston–cylinder arrangement.

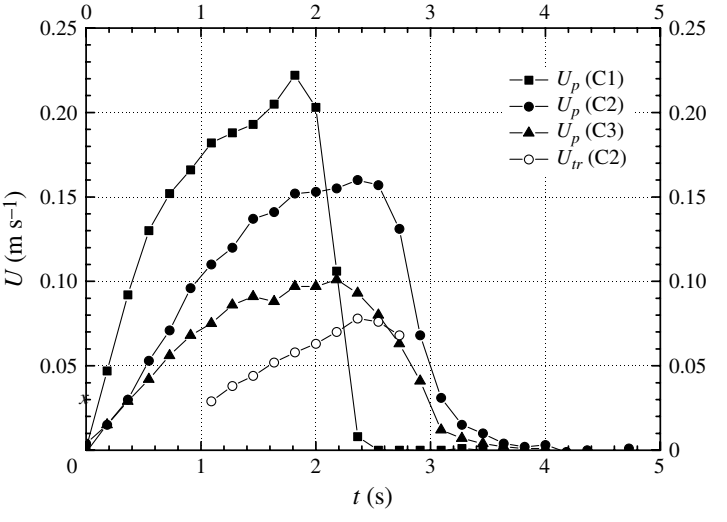

FIGURE 2. Piston velocity programs for the three cases at different Reynolds number and the translational velocity of the leading vortex ring in C2.

by Dantec, which have a mean diameter of 50 μm and a density of 1.03 g cm^{-3}, are chosen as the seeding particles. The particles are illuminated by a dual-cavity pulsed Nd:YAG laser (NewWave Gemini) with a maximum repetition rate of 15 Hz for each cavity. The maximum energy level is 120 mJ per pulse and the pulse duration is 10 ns. The emitted laser is green with a wavelength of 532 nm. A cylindrical lens is used to form a laser sheet with thickness of 3 mm and divergence angle of 32°, which is positioned vertically on the x–r plane. The 12-bit digital camera (HiSense MkII), to which the AF Micro Nikkor 60 mm lens is attached, is positioned normal to the

laser sheet plane and records the images of the particle field in the region bounded by $0 < x/D < 5.5$ and $-2 < r/D < 2$ with a spatial resolution of 1344×1024 pixels. Although the laser could achieve higher frequency, the actual measurements are taken at the frequency of 5.5 Hz due to the limit of the camera frame rate (maximum 5.6 Hz for the double-frame mode). The standard cross-correlation technique (Willert & Gharib 1991) is employed to obtain velocity field data from the PIV images. Using an interrogation area of 32×32 pixels and a step size for the moving average of 16×16 pixels (50 % window overlap), the processing can construct a flow field of 83×63 velocity vectors. In addition, vorticity fields are computed using finite differences of the velocity data at eight neighbouring points via a second-order accurate scheme. The uncertainties in the measured velocity and azimuthal vorticity results are estimated to be within 1 and 3 %, respectively (Gao *et al.* 2008).

It is important to note that the size of the seeding particles is chosen carefully because the accuracy of the velocity field measurement is limited by the ability of the seeding particles to follow the instantaneous motion of the fluid. Accordingly, a compromise between: (i) increasing the particle size so as to improve light scattering; and (ii) reducing the particle size to improve flow tracking is considered. First, for light scattering requirement, the camera images of seeding particles should have a diameter of at least 2 pixels, preferably 3 pixels or more. By applying this criterion to the present experiment in which pixel size of the camera b_p is 6.45 μm, it suggests that a seeding particle image should be at least $d_{image} = 2 \times b_p = 12.9$ μm. On the image plane, the diameter of the Airy disc encompassing the light scattered by the seeding particles is given approximately by

$$d_{image} \approx \left[\frac{d_p^2}{s^2} + \left(2.44 \left(1 + \frac{1}{s} \right) f\lambda \right)^2 \right]^{1/2}, \tag{2.2}$$

where d_p is the particle diameter, s is the scale factor, f is the f-number of the lens aperture and λ is the wavelength of laser (Adrian & Westerweel 2010). According to the conditions of the present experiment (i.e. $s = 15.9$, $f = 8$ and $\lambda = 0.532$ μm), it is found that the image of a 50 μm-diameter particle has a diameter of 11.5 μm, i.e. close to the requirement of 2 pixels. On the other hand, the size of seeding particles is restricted by its ability to follow the flow closely. For liquid flow, the upper limit on particle diameter is considerably more lenient than in gas flow, because of the much smaller density ratio. If $\rho_p/\rho_f = 1$ (ρ_p and ρ_f are the density of seeding particle and fluid, respectively), particles will follow the flow exactly regardless of the size (Hjelmfelt & Mockros 1966; Mei 1996). However, it is realized that in strong shear flow the dynamics of small particles are affected by the shear lift force. Saffman (1965, 1968) showed that the transverse lift force on the particle (*Re* is small compared with unity) is approximated by

$$f_L = 6.64\mu V \left(\frac{d_p}{2} \right)^2 \left(\frac{\kappa}{\nu} \right)^{1/2}, \tag{2.3}$$

where V is the instantaneous relative velocity, κ the magnitude of the velocity gradient and μ and ν dynamic viscosity and kinematic viscosity, respectively. To examine its influence on the motion of particles, a simple comparison between the lift force and the quasi-steady viscous force, which contributes to the tracking ability of particles, has been conducted. The viscous force is given by Stokes' drag law as

$$f_v = -3\pi\mu d_p V. \tag{2.4}$$

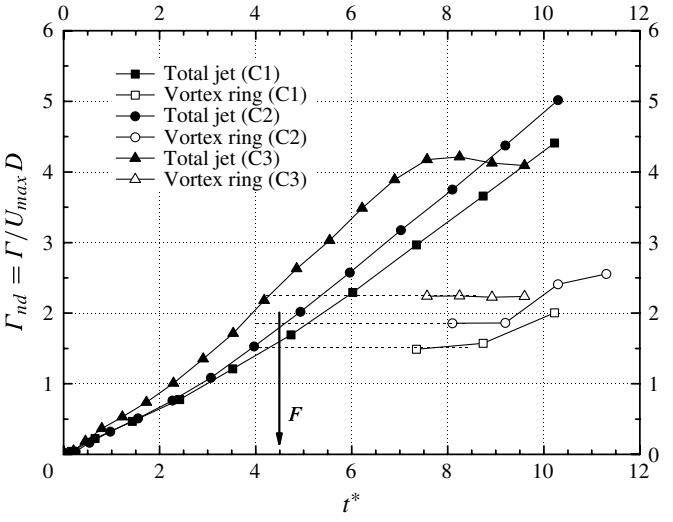

FIGURE 3. Normalized circulation of the total jet and the leading vortex ring as a function of formation time for the three cases.

It is interesting to note that the ratio $|f_L|/|f_v|$ is actually independent of the relative velocity V. According to the conditions of the present experiment (i.e. $d_p = 50$ μm) and by assuming that maximum velocity gradient is approximately $\kappa \approx 50\ \mathrm{s}^{-1}$ (similar to Gharib *et al.* 1998), the ratio of lift force and viscous drag is $|f_L|/|f_v| \approx 6\,\%$. This suggests that the motion caused by the transverse lift force is much smaller than the viscous resistance. Since Stokes' drag law gives a conservative estimate of the tracking ability of particles (Dring 1982), the influence of shear lift force could be even smaller than the present approximated estimation. Therefore, it can be shown that the neutral seeding particles of 50 μm mean diameter are capable of following the flow accurately and can be captured distinctly by the camera in the present experiment.

3. Experimental results and discussion

3.1. *Circulation of the leading vortex ring and the formation number*

As established by Gharib *et al.* (1998), determination of the formation number requires the evaluation of the circulation of the vortex ring after its pinch-off as well as the total circulation supplied by the jet generator. Before proceeding to further discussion, values for the formation number are first to be determined for the three cases. The variation of the total circulation and the vortex ring circulation, normalized by the maximum piston velocity U_{max} and nozzle diameter D, against the dimensionless formation time t^* is plotted in figure 3. The total circulation is obtained by integrating the vorticity contained within the lowest detectable contour level, which is determined to be at $3.0\ \mathrm{s}^{-1}$. Sensitivity analysis has been conducted by selecting different contour levels at 4.0, 3.0 and $2.0\ \mathrm{s}^{-1}$ as the boundary of the vortex ring. The circulation of the leading vortex ring is found to be sensitive to the choice of the cut-off level between 4.0 and $3.0\ \mathrm{s}^{-1}$, especially in the time after the leading vortex ring has pinched-off. Below $2.0\ \mathrm{s}^{-1}$, the noise signal becomes unacceptable. As such, the vorticity contour level at $3.0\ \mathrm{s}^{-1}$ is chosen for the present experiment.

Figure 3 shows that the total circulation of the starting jet increases monotonically against the formation time. The circulation of the leading vortex rings can only be calculated after the complete separation of their vorticity field from the trailing jet ($t^* > 7.0$). The dimensional circulation of the leading vortex rings after the pinch-off is found to be at the level of approximately 84, 77 and 61 $cm^2\ s^{-1}$ for cases C1, C2 and C3, respectively. As shown by the dashed lines in figure 3, the corresponding formation numbers are found to be approximately 4.5 ± 0.1 for C1 and C2, and a little smaller value of 4.2 for C3. These results are in agreement with the formation number reported by Gharib *et al.* (1998) for the cases with similar non-impulsive velocity programs.

3.2. *Characteristics of the secondary vortices during the pinch-off*

The development of secondary vortices in the trailing jet is examined in terms of the evolution of the vorticity contours in the flow field, as shown in figure 4 for C2. In general, as the formation time increases, the leading vortex ring grows in size and strength by absorbing the fluids and vorticity from the trailing jet, and translates downstream due to self-induction. At large formation time, secondary vortices, i.e. the large-scale coherent structures characterized by organized vorticity distribution, are gradually formed in the trailing shear layer. The vorticity field of the leading vortex ring remains connected to that of the trailing jet after the formation number, indicating that the leading vortex ring continues to absorb fluids and gain vorticity from the generating jet. The pinch-off process completes when the physical separation between the leading vortex ring and the trailing jet happens at $t^* \approx 8$. This suggests that the entire pinch-off process requires 3–4 formation time units to complete for C2. Similar values for the separation time have also been found for C1 (7.5 ± 0.2) and C3 (8.2 ± 0.2). These results imply that the separation time in a starting jet may be delayed by lowering the Reynolds number.

From the evolution of the vorticity contours, it is also observed that variation of the separation time among the three cases is associated with the formation of the secondary vortices and their interaction with the leading vortex ring. For C2, an initial concentrated distribution of vorticity, which gradually evolves into the first trailing vortex (V1), can be distinguished in the trailing jet near the nozzle exit at $t^* = 4.9$, as shown in figure 4(*c*). As the starting jet continues, the first trailing vortex shrinks in the radial extent and subsequently accelerates forward through the centre of the leading vortex ring (see figure 4*d*). This process in fact is very similar to the leap-frogging behaviour for two coaxial vortex rings travelling in the same direction (Maxworthy 1972; Riley & Stevens 1993; Lim 1997). In the present experiments, however, the first trailing vortex is actually entrained into the leading vortex ring (as shown by the distorted structure in the vorticity contours of the leading vortex ring in figure 4*e*), instead of catching up with the leading vortex ring and then emerging in front of it like in the leap-frogging process. This is mainly due to the fact that the first trailing vortex is much weaker, in terms of its size and circulation strength, than the leading vortex ring. It is noted that, in C2, the first trailing vortex cannot develop fully into a tight spiral consistent with the formation of a new vortex ring (such as the second trailing vortex (V2) at $t^* = 8.1$) due to the vortex merging. The vortex merging process between the leading vortex ring and the first trailing vortices has also been observed by O'Farrell & Dabiri (2010) based on the Lagrangian coherent structures (LCSs).

As a result of the vortex merging, the circulation of the first trailing vortex is absorbed by the leading vortex ring. This suggests that vortex merging would serve

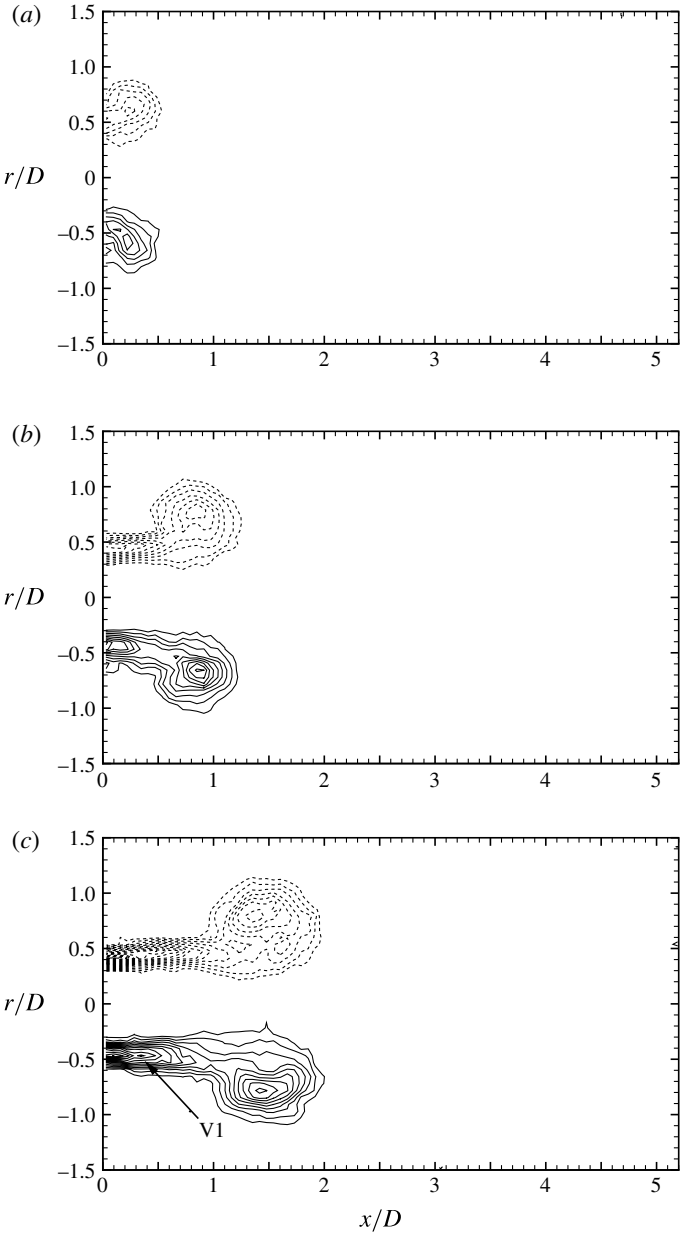

FIGURE 4. For caption see the next page.

to speed up the process of the leading vortex ring accumulating circulation, which, otherwise, is only transported by the continuous vorticity flux from the trailing shear layer. As such, the leading vortex ring will gain the maximum circulation and separate from trailing jet earlier than the cases without vortex merging during the pinch-off process. Because the trailing vortex ring acts as a large disturbance, the vorticity distribution within the core of the leading vortex ring would be rearranged towards its equilibrium state (approximated as the Norbury–Fraenkel family of vortex rings). In C1, the vortex merging of the leading vortex ring and the first trailing vortex happens

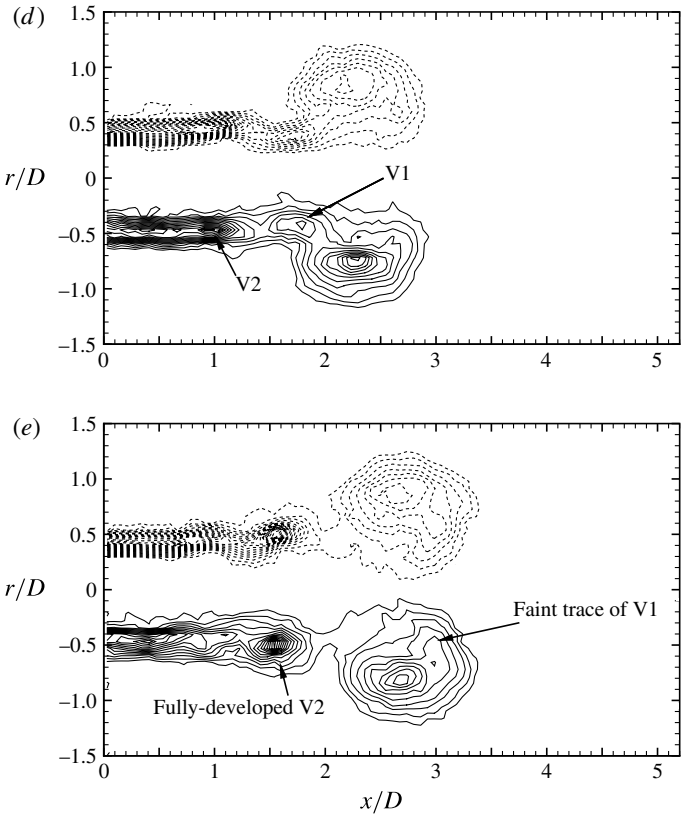

FIGURE 4. (contd). Temporal evolution of vorticity field for C2: (*a*) $t^* = 1.0$; (*b*) $t^* = 3.1$; (*c*) $t^* = 4.9$; (*d*) $t^* = 7.0$; and (*e*) $t^* = 8.1$.

slightly earlier than in C2. However, the vortex merging is not observed before the end of the pinch-off process in C3 at lower Reynolds number.

Different behaviour of the vortex merging process for the three cases is actually associated with the development of secondary vortices at different Reynolds number and velocity program. The trajectories of the first and second trailing vortices are plotted in figure 5 for the three cases. The first trailing vortex can firstly be distinguished by the vorticity contours at formation time $t^* \approx 4.8$ and at the axial position of $x/D \approx 0.35$. Subsequently, trajectories of the trailing vortices for the three cases show that decreasing the Reynolds number of the starting jet affects the convection of both the first and second trailing vortices slightly. Because the trailing vortices translate slower at smaller Reynolds number, the distance between the leading vortex ring and first trailing vortex becomes greater, as shown in figure 6. Therefore, the interaction between them, which leads to the vortex merging process, becomes weaker. It is also shown in figure 5 that the first trailing vortex in C1 and C2 disappears after $t^* \approx 6$ and 7, respectively, because they have been merged into the core of the leading vortex ring. For these two cases, the second vortex merging process (between the new leading vortex ring and the second trailing vortex) happens later at around $t^* = 8.8$ in C1 and $t^* = 10.3$ in C2. On the other hand, the first trailing vortex in C3 develops fully into tight spirals and persists in the trailing jet even after the end

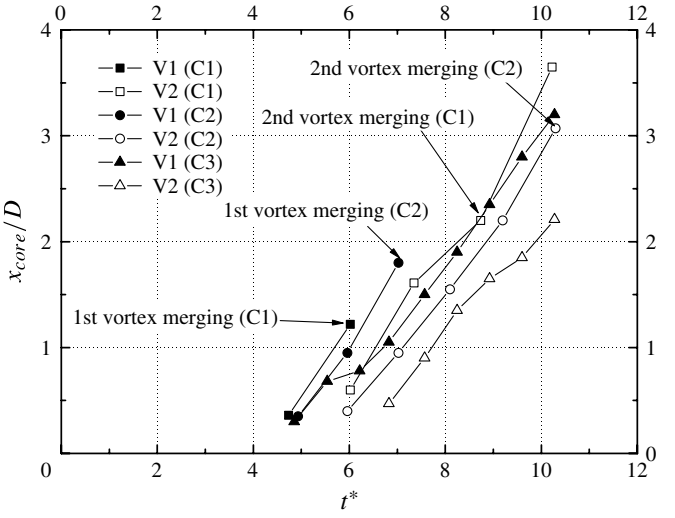

FIGURE 5. The trajectory of the first (V1) and second (V2) trailing vortex rings.

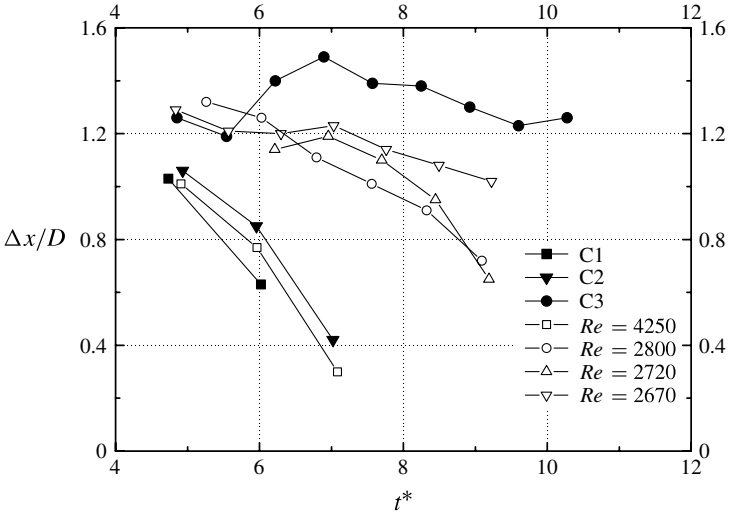

FIGURE 6. The variation of axial distance between the leading vortex ring and the first trailing vortex ring (V1) against the formation time. Other cases in the present experiment are also included.

of the pinch-off process. Results at larger formation time ($t^* > 8$) shows that the first vortex merging in C3 occurs as late as $t^* \approx 11$.

Based on the above discussion, it can be concluded that the secondary vortices are formed in the trailing jet only after the formation number, and its subsequent interaction with the leading vortex ring affects the physical separation between the two parts by means of vortex merging. As the development of the secondary vortices is dependent on the Reynolds number of the starting jet, a higher Reynolds number leads

to a faster translation of trailing vortices and stronger vortices interaction, which in turn accelerates the separation of the leading vortex ring from its trailing jet.

3.3. *Vorticity and momentum fluxes*

To examine the effect of the initial roll-up and the subsequent development of the secondary vortices on the pinch-off process, the variation of axial vorticity and momentum fluxes, which are defined in the ground coordinate system as

$$\frac{\mathrm{d}\Gamma}{\mathrm{d}t} = \int_0^\infty \omega(x, r)u(x, r)\,\mathrm{d}r, \tag{3.1a}$$

and

$$\frac{\mathrm{d}M}{\mathrm{d}t} = \int_0^\infty 2\pi\rho u^2(x, r)r\,\mathrm{d}r, \tag{3.1b}$$

are calculated for C2. The integration is conducted by a fourth-order-accurate quadrature scheme at every axial position.

Their axial variations during the initial formation stage and pinch-off process are plotted in figure 7. As shown in figure 7(*a*), the vorticity flux decreases slightly from the nozzle exit to a minimum just behind the leading vortex ring before the formation number ($t^* = 3.1, 4.0$), due largely to viscous diffusion. During the pinch-off process ($t^* = 4.9$), the decrease in vorticity flux behind the leading vortex ring becomes more appreciable. By $t^* = 6.0$, the second peak of vorticity flux behind the leading vortex ring can be identified, corresponding to the roll-up of the first trailing vortex. As discussed in the previous section, the first trailing vortex will be entrained into the leading one due to their interaction (see figure 4*d*). Thus, the second peak in vorticity flux disappears at $t^* = 7.0$ and the minimum point in the vorticity flux is followed immediately by the second trailing vortex, while the first trailing vortex is being entrained by the leading vortex ring. When the vortex merging process completes ($t^* = 8.1$), a sharp second peak appears at $x/D \approx 1.5$ and the vorticity flux behind the leading vortex ring almost vanishes, suggesting that the second trailing vortex is accumulating vorticity around itself. Since no more vorticity will be added into the leading vortex ring, it has achieved the maximum circulation and its growth has terminated by the separation time.

The corresponding evolution of the momentum flux is presented in figure 7(*b*). The momentum flux in the trailing jet seems almost constant even after the onset of the pinch-off process ($t^* \approx 4.9$). Comparing with the vorticity flux at this instant, the effect of the first trailing vortex on the momentum flux is not as significant. However, at $t^* \geqslant 6.0$, the momentum flux starts having a minimum point behind the leading vortex ring, indicating the initial roll-up of the second trailing vortex. By $t^* = 8.1$, the second peak of momentum flux becomes obvious in the trailing jet, which actually corresponds to the second trailing vortex (as already shown in figure 4). In the models for the pinch-off process proposed by Shusser & Gharib (2000) and Gao & Yu (2010), the trailing jet is approximated as a one-dimensional axisymmetric flow with constant mass and momentum flux. The present experimental result demonstrates that this approximation should only be applied at the initial vortex ring formation stage (i.e. $t^* \leqslant F$), and the conservation of momentum fails after the formation of trailing vortices. In addition, by comparing figure 7(*a*) with figure 7(*b*), it is shown that the vorticity flux is actually more susceptible to the formation and growth of the secondary vortices than the momentum flux.

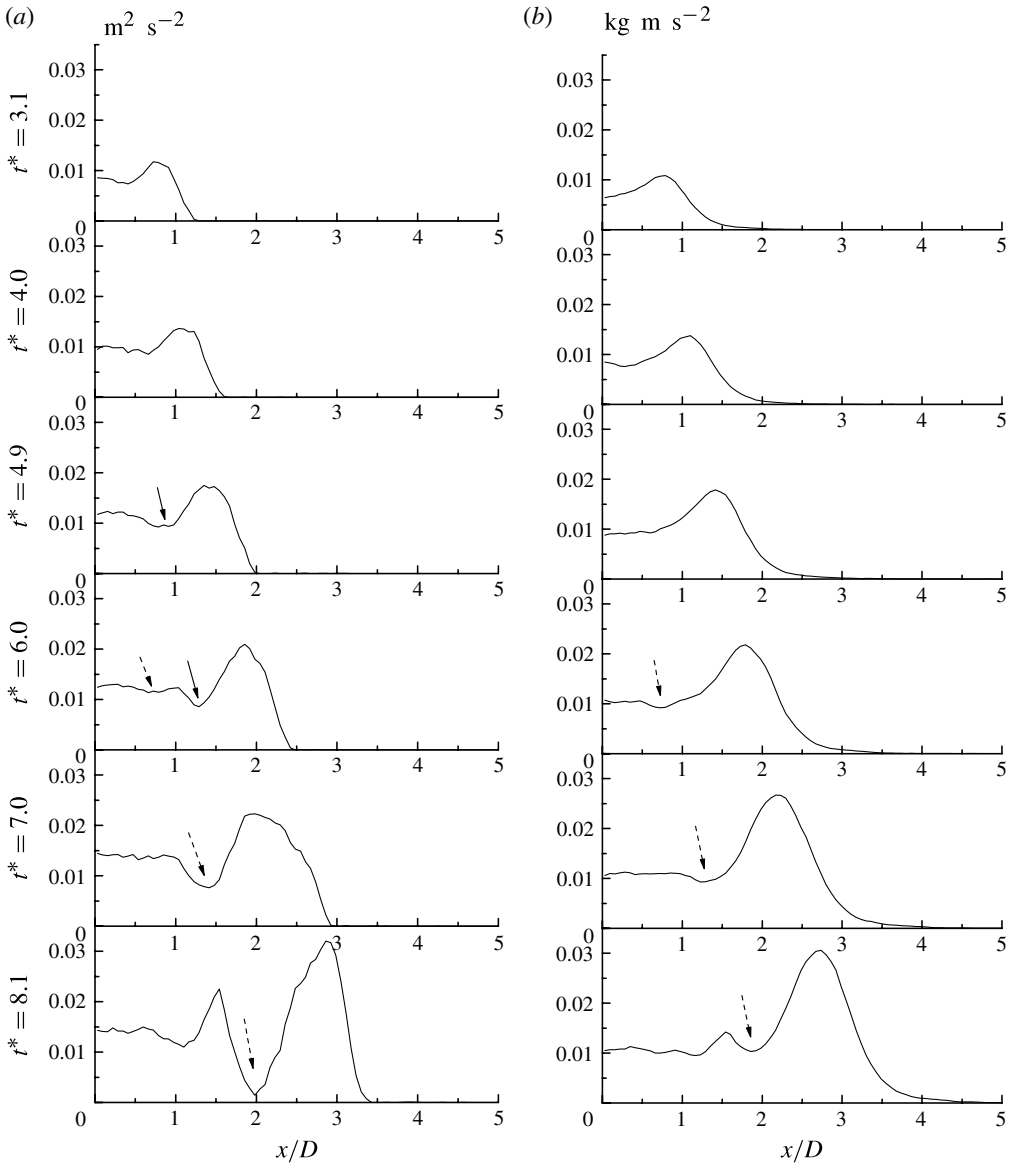

FIGURE 7. Axial variation of the absolute vorticity and momentum fluxes during the pinch-off process for C2. Arrows with a solid line indicate the boundary between the first trailing vortex (V1) and the leading vortex ring, and arrows with a dashed line indicate the boundary between the first (V1) and second (V2) trailing vortices: (*a*) vorticity flux; and (*b*) momentum flux.

Based on the dynamics of the pinch-off process elucidated by Mohseni *et al.* (2001), the leading vortex ring is fed by the trailing shear layer at a specific rate, which actually determines the final state of the leading vortex ring. Owing to the development of secondary vortices in the trailing jet, the rate at which the vorticity and momentum are being delivered into the leading vortex ring is affected. By taking into account the translational velocity of the leading vortex ring, the local effect of trailing

jet instability on the net vorticity and momentum flux added into the leading vortex ring is examined. The vorticity and momentum fluxes relative to the translation of the leading vortex ring are calculated at its boundary with the trailing jet as

$$\left.\frac{\mathrm{d}\Gamma}{\mathrm{d}t}\right|_r = \int_0^{r_1} \omega(x, r)[u(x, r) - U_{tr}]\,\mathrm{d}r, \tag{3.2a}$$

and

$$\left.\frac{\mathrm{d}M}{\mathrm{d}t}\right|_r = \int_0^{r_1} 2\pi\rho u(x, r)[u(x, r) - U_{tr}]r\,\mathrm{d}r, \tag{3.2b}$$

respectively, where the translational velocity U_{tr}, shown in figure 2, is estimated by tracking the position of the maximum vorticity in the vortex ring core and r_1 is the radial position where the local axial velocity drops to the translation velocity, i.e. $u = U_{tr}$. The boundary of the leading vortex ring is defined as the position of minimum vorticity flux immediately behind the leading vortex ring as shown in figure 7(*a*). It is noted that during the vortex merging process, the boundary is determined approximately by the shape of the leading vortex ring (at $x/D \approx 1.65$ in figure 4*d*, for example), so as to exhibit the effect of the sudden increment of vorticity and momentum by entraining the secondary vortex.

The relative vorticity and momentum fluxes for C2 are plotted against the formation time in figure 8. Although the general trends for both vorticity and momentum fluxes are similar, their quantitative behaviours are different. The initial acceleration of the piston has more appreciable effect on the momentum flux than the vorticity flux. After the formation number is reached, the vorticity flux starts to decrease gradually up to $t^* \approx 6$ under the influence of the first trailing vortex, while the momentum flux still continues to increase albeit with decreasing rate. The sudden jump in the vorticity flux at $t^* \approx 7$ is attributed to the vortex merging process that takes place between the leading vortex ring and the first trailing vortex. The momentum flux is only slightly affected by the merging process, due to the fact that the first trailing vortex is not fully developed and has little influence on the irrotational flow around itself. When the vortex merging process completes, the vorticity flux drops sharply to almost zero at $t^* \approx 8$, corresponding to the end of the pinch-off process. Figure 8 shows further that there is still momentum (and also kinetic energy) being transported into the leading vortex ring after the separation time. Hence, one may speculate that the growth of the leading vortex ring is maintained mainly via the vorticity flux conveyed by the trailing shear layer, rather than the flux of momentum or kinetic energy. The rapid decrease in vorticity flux implies that the rotational fluids in the trailing shear layer can no longer be fed into the core of the leading vortex ring, but rather be accumulated in a series of forming trailing vortices. The remaining momentum flux after pinch-off suggests that the irrotational fluids in the potential core of the trailing jet, which carry linear momentum and kinetic energy only, could still enter the vortex ring bubble, but staying outside the vortex ring core. Thus, the leading vortex ring ceases to grow and gradually approaches its equilibrium state. Moreover, the second peak of both fluxes at $t^* \approx 10.3$ corresponds to the subsequent vortex merging between the pinched-off vortex ring and the second trailing vortex. The momentum flux into the leading vortex ring eventually vanishes at $t^* > 11$ when the formation of subsequent secondary vortices becomes dominant in the trailing jet.

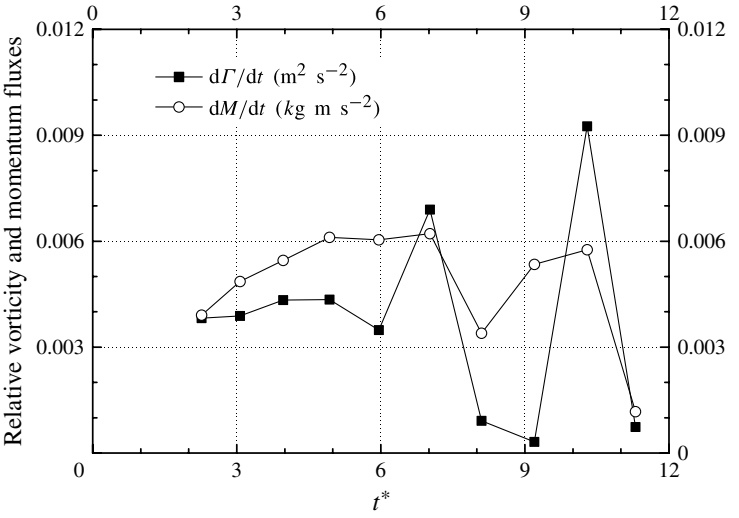

FIGURE 8. Fluxes of momentum and vorticity fed into the leading vortex ring during its formation and pinch-off process. The cutting level for the calculation of vorticity flux is 3.0 s^{-1}.

4. The instability of shear layer in the trailing jet

The shear layer is inviscidly unstable to infinitesimal perturbation via the Kelvin–Helmholtz instability mechanism. It is shown in § 3 that the secondary vortices are formed in the trailing jet only after the formation number. Their growth somehow decreases the vorticity flux being fed into the leading vortex ring, leading to the complete separation between the two parts. Given the temporal sequence between the formation number and the secondary vortices roll-up, in this section we investigate the instability characteristics of the trailing shear layer before and during the pinch-off process in order to find out factors that affect the initial formation of the secondary vortices.

The initial development of the shear layer downstream of the nozzle edge is dominated by a linear stability mechanism, owing to the infinitesimal amplitude of the perturbation in the main flow. The linear stability theory indicates that momentum thickness of the shear layer is an important parameter to determine the instability characteristics of an axisymmetric shear layer. The momentum thickness θ is defined as

$$\theta(x) = \int_0^\infty \frac{u(x,r)}{U_c(x)}\left(1 - \frac{u(x,r)}{U_c(x)}\right) \mathrm{d}r, \tag{4.1}$$

where $U_c(x)$ is the centreline velocity at each axial position x. Figure 9(*a–c*) present the momentum thickness of the trailing shear layer as a function of streamwise coordinate x/D during the vortex ring formation process for the three cases. For C1 and C2, it can be observed that θ increases rapidly in the streamwise direction before the formation number. For example, at $t^* = 3.5$, θ in C1 increases by as much as 80 % near the nozzle exit (from $x/D = 0.03$ to $x/D = 0.5$). However, at $t^* > 5$, θ only increases slightly or remains constant within the range of $0 < x/D < 0.5$. For a continuous jet at $Re \approx 2.7 \times 10^4$, Cohen & Wygnanski (1987) found that, for $x/D \leqslant 0.45$, the shear layer is almost parallel and all its velocity profiles are

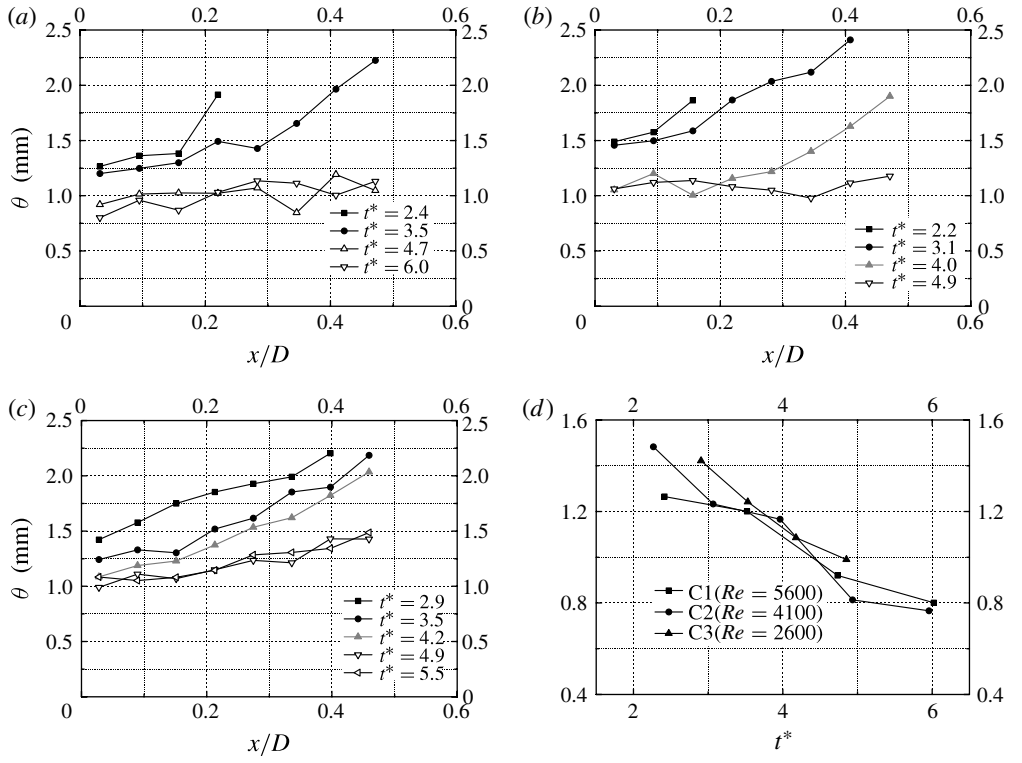

FIGURE 9. Axial variation of the momentum thickness at several formation times for: (*a*) C1; (*b*) C2; and (*c*) C3. (*d*) The variation of the initial momentum thickness at nozzle exit ($x/D \approx 0.03$) as a function of the formation time.

self-similar, but it spreads rapidly farther downstream ($1 \leqslant x/D \leqslant 4$). Therefore, the behaviour of the shear layer after the formation time resembles that of a continuous jet. It is interesting to note that at $t^* = 4.0$ in figure 9(*b*), the streamwise variation of momentum thickness exhibits a trend of the transition between the two patterns. Despite a slight fluctuation, the momentum thickness can be regraded as a constant at region very close to the nozzle ($0 < x/D < 0.2$), but it increases at a steeper slope for $x/D > 0.3$, i.e. similar to the variation before the formation number. This observation implies that the change in the spreading pattern of the trailing shear layer around the critical formation time should have some impact on the development of spatially growing perturbations in the shear layer, as well as their roll-up into secondary vortices during the pinch-off. On the other hand, the change in the streamwise increase of θ becomes less obvious in C3. As shown in figure 9(*c*), θ still increases at a gentler slope even when t^* becomes greater than the formation number. This behaviour of the shear layer may stem from the more appreciable viscous diffusion effect at lower Reynolds number. It is also necessary to point out that the reduction of initial momentum thickness (as shown in figure 9*d*) is the direct result from the acceleration of the piston motion, rather than being the generic feature of the starting jet. In contrast, the initial momentum thickness of the shear layer actually increases as jet ejection continues, due to the growth of the boundary layer on the inner wall of the nozzle (Shusser *et al.* 2002).

The effect of the momentum thickness on the instability of the axisymmetric shear layer has been investigated by Michalke (1971), Morris (1976) and Michalke & Hermann (1982) by means of the inviscid linearized stability theory. It is found that with increasing $\theta/R_{1/2}$ ($R_{1/2}$ is the centre of the shear layer where the axial velocity u drops to a half of the centreline velocity U_c), the axisymmetric shear layer becomes less unstable, i.e. having smaller maximum amplification rate for the spatially growing perturbation. Meanwhile, the frequency of the most amplified perturbation wave, usually referred to as 'the natural frequency', shifts towards lower values. In the case of an unforced jet, such as the present experiment, the initial excitation is introduced by natural disturbance in the main flow. Only the perturbations at frequency close to the natural frequency are 'selected' to develop into discrete vortices. According to results shown in figure 9(*a–c*), the spatially growing perturbation before the formation number is amplified at a decreasing rate and there is not a consistent natural frequency to support the selective amplification because the shear layer spreads rapidly while being convecting downstream. Therefore, the initially infinitesimal perturbation waves cannot be amplified sufficiently in the shear layer to approach the nonlinear instability regime, in which discrete vortices could start to roll-up. On the other hand, due to the almost parallel shear layer after the formation number, perturbations near the corresponding natural frequency can be amplified and evolve into secondary vortices at the downstream location. Based on the effect of momentum thickness of a shear layer on its instability characteristics, the present results suggest that the very slow spread of the shear layer should be taken as an important factor for the roll-up of secondary vortices only after the formation number.

Another factor that affects the initial roll-up of secondary vortices is the finite streamwise dimension of the trailing shear layer. Todde, Spazzini & Sandberg (2009) indicated that the distance from the exit plane required for the roll-up of the vortices is influenced by the Reynolds number and the boundary layer thickness at the nozzle exit. According to their flow visualization results for a continuous jet at Reynolds number of 2700 (see figure 18 in their paper), the growth of the instability waves is hardly identified at about $x/D < 0.8$. For the starting jet in the present study, the length of the trailing shear layer, which is defined as the distance from the nozzle exit to the location of minimum vorticity flux immediately behind the leading vortex ring (i.e. the rear boundary of the leading vortex ring defined in § 3.3), is shown in figure 10. In general, variations of the length of the trailing jet for the three cases are almost the same, except that C3 has slightly longer trailing shear layer than the other two cases. It is also observed that before the formation number the streamwise dimension of the trailing shear layer is approximately less than $0.8D$ for C3, and less than $0.7D$ for C1 and C2. These values of trailing jet length are very close to the distance required for the initial roll-up of vortices in a continuous jet. Based on the above reasoning, it can be conjectured that in the initial stage of a starting jet, the perturbations in the trailing shear layer would be absorbed into the leading vortex ring before it can evolve into a compact coherent structure. Therefore, the secondary vortices are formed only after the formation number.

In a starting jet, it is appropriate to relate the change of the instability characteristics of the trailing shear layer to the influence of the leading vortex ring. First, it is obvious that the dimension of the trailing shear layer is determined by the streamwise translation of the leading vortex ring. The perturbation waves can evolve into compact

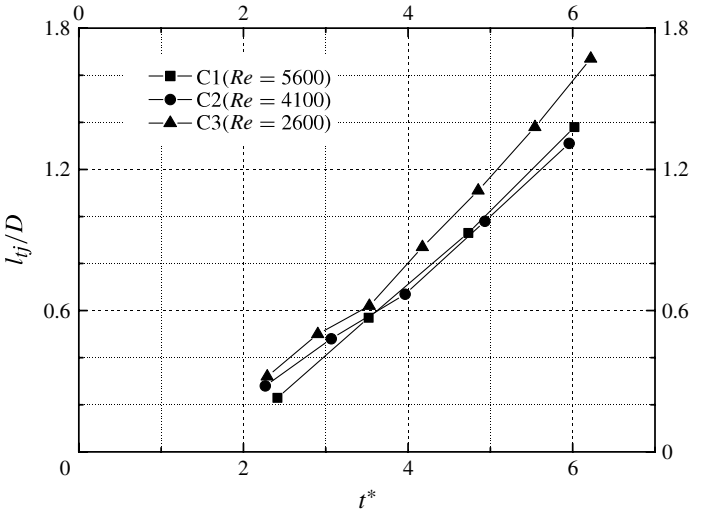

FIGURE 10. The streamwise length of the trailing shear layer as a function of the formation time for the three cases.

secondary vortices only when the leading vortex ring translates further downstream. Second, the variation of shear layer expansion should be associated with the induced radial velocity by the leading vortex ring. According to the Biot–Savart law, the rotational fluid in the leading vortex ring core induces inward radical velocities in its immediate upstream vicinity. As shown in figure 11(*a*), at $t^* = 3.1$ the trailing shear layer (at $x/D < 0.5$) is subjected to the influence of the induced velocity field. Because the inward radial velocity field pushes the ambient fluids towards the trailing shear layer, the exchange of momentum between the ejected fluid in the trailing jet and the ambient fluid with relatively slow velocity are enhanced. As a result, the velocity profiles in the shear layer spread out radially. Since the magnitude of induced velocity diminishes as the distance of the leading vortex ring relative to the nozzle exit increases, its effect on shear layer expansion decreases consequently. By $t^* = 4.9$ when the vortex ring core travels downstream to approximately $x/D = 1.4$, as shown in figure 11(*b*), the induced radial velocities become almost negligible (less than 4 % of the local axial velocity) near the jet exit. Without the expanding effect from the leading vortex ring, the trailing shear layer will be maintained almost parallel and the amplification rate of perturbation will not be diminished as they are being convected downstream.

In short, the leading vortex ring exerts a stabilizing effect on the shear layer behind it before the formation number, via its induced radial velocities and its axial translation. As the leading vortex ring travels downstream away from the nozzle exit, its effect on the trailing shear layer becomes weaker, especially near the nozzle exit. At the same time, the length of the shear layer keeps increasing, resulting in the roll-up of the secondary vortices after the formation number. Further growth of the secondary vortices leads to the decrease in the vorticity flux being fed into the leading vortex ring and, finally, results in their physical separation. The above analysis, therefore, suggests that in a starting jet, the development of the instability of the trailing shear layer should be regarded as a determinant factor that limits the growth of the leading vortex ring with larger circulation.

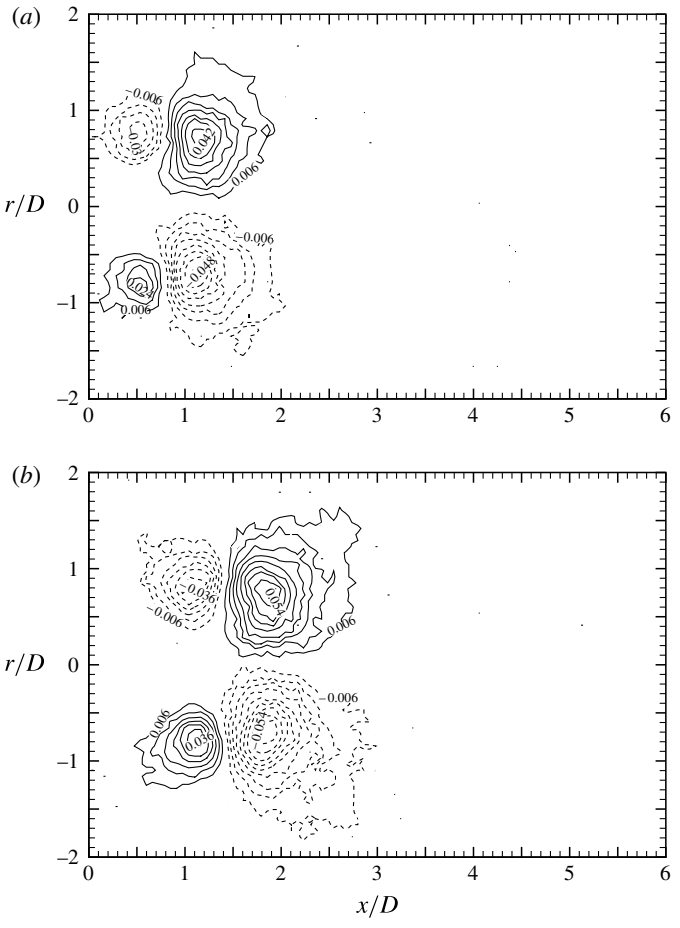

FIGURE 11. Contours of the radial velocity before and during the pinch-off process: (*a*) radial velocity contours before pinch-off ($t^* = 3.1$); and (*b*) radial velocity contours during pinch-off ($t^* = 4.9$).

5. Pinch-off criterion in terms of the trailing jet instability

With the understanding of the significant role of the trailing jet instability in the pinch-off process, we intend to discuss an alternative criterion for the onset of the pinch-off process in starting jets. It is based on the explanation of the pinch-off process in terms of the development of trailing jet instability and the interaction between the leading vortex ring and the secondary vortices.

5.1. *The physical process of vortex ring pinch-off*

The experimental results suggest that the limiting process of vortex ring formation can be understood from the perspective of the unstable trailing shear layer development, i.e. the formation and the subsequent evolution of the secondary vortices. Therefore, it is important to first discuss the physical implication of the formation number in terms of the development of the trailing shear layer instability.

The evolution of a starting jet at different stages of the pinch-off process is illustrated schematically in figure 12. In order to focus on the main physical aspects,

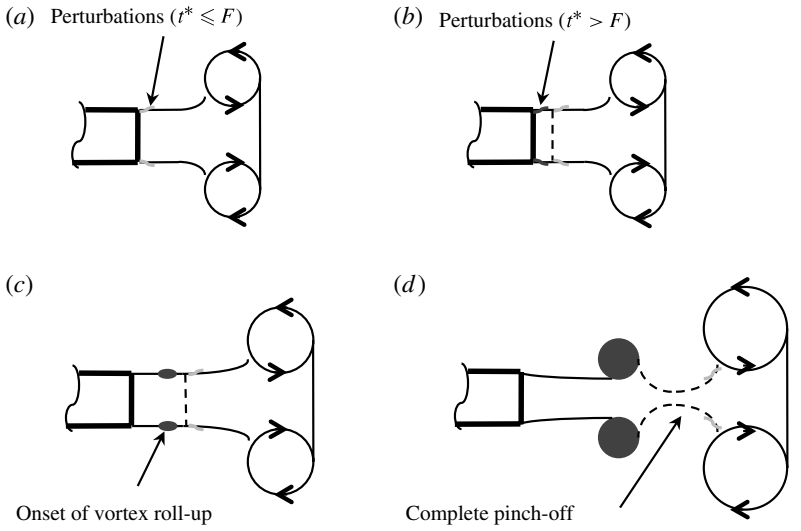

FIGURE 12. Sketch of the development of infinitesimal perturbations in the trailing shear layer during the pinch-off process: (*a*) at the formation number; (*b*) slightly after the formation number; (*c*) during the pinch-off process; and (*d*) at separation time.

we consider first a pinch-off process without vortex merging, such as C3. Up to the formation number (figure 12*a*), the leading vortex ring grows in size and strength via the continuous vorticity influx from the trailing jet, and at the same time translates downstream due to self-induction. According to the definition of the formation number, only the vorticity emanating from the nozzle before this critical time can be accumulated in the leading vortex ring. Thus, there should be an imaginary boundary in the trailing shear layer which distinguishes between the fluids issued before and after the formation number, as indicated by the dashed line in figure 12(*b*,*c*). The natural perturbation in the shear layer emanated before or at the formation number (in light grey) cannot be amplified enough to roll-up into a vortex due to the induced velocity field of the leading vortex ring and the short length of the trailing shear layer. It will instead be entrained by the leading vortex ring during the pinch-off process (figure 12*d*). On the other hand, due to the critical change in the instability characteristics of the trailing shear layer, the perturbation emanated after the formation number (in darker grey) can be amplified sufficiently to roll-up into a secondary vortex (figure 12*c*). As the secondary vortex grows, it continuously absorbs vorticity around itself, which leads to the complete pinch-off at the separation time (figure 12*d*).

It is noted that the pinch-off process with vortex merging, such as C1 and C2, manifests the same dynamic process of instability development as that without vortex merging, but the shear layer is more unstable (due to a higher Reynolds number, for example). In these cases, the perturbations emanated just before the formation number can still roll-up into secondary vortices. However, due to the vortex merging process, the first secondary vortex cannot develop fully into a tight spiral and persist in the trailing shear layer during the pinch-off process. Only the secondary vortex that is formed immediately after the first one can develop fully into a tight spiral in the trailing shear layer, decreasing the vorticity flux being fed into the leading vortex ring.

The evolution of the secondary vortex that merges with leading vortex ring during the pinch-off can be regarded as the transitional behaviour between the suppressed

perturbations issued before the formation number and the fully developed secondary vortices in the trailing shear layer, as shown in the case without vortex merging. Given the difference in vorticity increment by the trailing shear layer and by a secondary vortices, the vortex merging during pinch-off should be a good explanation for the 20 % variations in the leading vortex ring circulation and the formation number at different Reynolds number and initial shear layer thickness reported by Zhao *et al.* (2000).

According to the description of the instability development of the trailing shear layer, the formation number should correspond to the moment when the perturbations that can later evolve into the first fully developed secondary vortex is about to be issued from the nozzle exit. Since this secondary vortex will not be absorbed by the leading vortex ring during the pinch-off process, its initial form (the corresponding infinitesimal perturbation) is indicative of a new vortical structure in the trailing jet. Thus, the physical implication of the formation number is actually consistent with experimental result of O'Farrell & Dabiri (2010) that the formation number coincides with the appearance of a new LCS near the nozzle edge.

5.2. *A criterion for the formation number*

The formation of the leading vortex ring is restricted by the growth of the secondary vortices in the trailing jet. This suggests an approach to characterize the limiting process of vortex ring formation by considering the evolution of infinitesimal perturbations in the trailing shear layer.

As discussed in § 4, the roll-up of the secondary vortices is affected by the induced velocity field and the downstream translation of the leading vortex ring. Therefore, parameters related to the trailing shear layer instability could be identified in terms of these two factors. Theoretically, for incompressible flow, the velocity field $\boldsymbol{u}(\boldsymbol{x})$ induced by a specific vorticity distribution $\omega(\boldsymbol{x})$ is expressed as

$$\boldsymbol{u}(\boldsymbol{x}) = \frac{1}{4\pi}\int \frac{\omega(\boldsymbol{x}')\times \boldsymbol{r}}{r^3}\,\mathrm{d}\boldsymbol{x}', \tag{5.1}$$

where $\boldsymbol{r} = \boldsymbol{x} - \boldsymbol{x}'$ and $r = |\boldsymbol{r}|$ (Saffman 1995). Equation (5.1) suggests that the induced radial velocity v_i depends on its axial distance to the core region of the leading vortex ring, and the magnitude and distribution of vorticity in the leading vortex ring. In a starting jet, however, it is difficult to determine the vorticity distribution of a unsteady vortex ring analytically during its formation stage. With appropriate simplification, the details of the vorticity magnitude and distribution in the leading vortex ring can be accounted for by its integration, i.e. the circulation. Hence, the induced radial velocity near the nozzle exit is determined by two parameters, namely the axial location of the vortex ring core x_{core} and its circulation Γ_{ring}. For the second factor affecting the trailing jet instability, the length of the trailing jet l_{tj} is also related to x_{core} due to their geometric relation. Finally, it is well known that the instability of the axisymmetric shear layer is dependent on the strength of the shear layer, i.e. the velocity difference ΔU between the jet and ambient fluids. The greater the velocity difference, the more unstable the shear layer becomes.

Based on these parameters that affect the instability of the trailing shear layer, dimensional analysis is conducted to determine the dimensionless parameters related to evolution of perturbation in the trailing shear layer. Its evolution can be characterized by its final amplification ratio R_a at the end of the pinch-off process, which is regarded as the ratio of the final amplitude to the initial amplitude of the perturbation. The variables associated with R_a include the circulation of the leading vortex ring Γ_{ring}, the

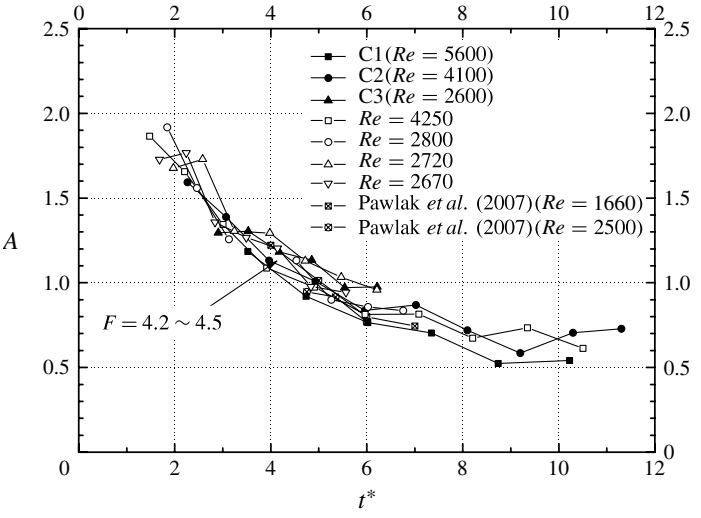

FIGURE 13. The variation of the parameter A against the formation time for the three cases. Results of other cases and of Pawlak *et al.* (2007) are also included.

axial trajectory of its core x_{core} and the strength of the shear layer ΔU (equal to U_0 when the jet is issued into a quiescent ambient fluid). Therefore, the expression for the final amplification ratio R_a can be written as

$$R_a = f(v_i, l_{ij}) = f(\Gamma_{ring}, x_{core}, \Delta U). \tag{5.2}$$

Using dimensional analysis, R_a is found only to depend on a single dimensionless parameter, referred to as A here, i.e.

$$R_a = f\left(\frac{\Gamma_{ring}}{x_{core}\Delta U}\right) = f(A). \tag{5.3}$$

This functional relation implies that the amplification of perturbation in the trailing shear layer is determined only by the value of the dimensionless parameter A.

The variation of the parameter A against the formation time for the three cases is plotted in figure 13. In the calculation of A, the trajectory and the integration region for circulation are obtained from a continuous sequence of vorticity contours for the starting jets. It is noted that for the unsteady vortex ring which is still connected to the trailing jet, its rear boundary (as defined in § 3.3) is used to distinguish its own vorticity field from that of the trailing shear layer. The results of Pawlak *et al.* (2007) and four other cases of the present experiment with different Reynolds number are also presented in figure 13 for comparison. Within the accuracy of the experimental data, it seems that the curves of A for the three cases are almost identical. As the formation time proceeds, A decreases monotonically. The physical implication of A is that it represents the capability of the leading vortex ring to suppress the exponential growth of the perturbation waves in the shear layer to approach the nonlinear development regime. The greater the value of A is, the less unstable the trailing shear layer becomes.

According to the interpretation of the formation number in terms of the development of the trailing shear layer instability, the critical value of A (A_c), corresponding to issuing the initial perturbation of the first fully developed secondary vortex from the

nozzle, is estimated by the formation number found in the present experiments. It is shown in figure 13 that A is approximately equal to 1.1 ± 0.1 for the three cases at their respective formation number $F = 4.2 \sim 4.5$. After the formation number, the values of A for respective cases drop below the critical value A_c. Noting that the present preliminary result of the critical value for A could be refined if it can be derived analytical by means of the hydrodynamic stability analysis and the solution for the induced velocity of the leading vortex ring. It is an interesting topic for further study. This quantitative result regarding to the trailing jet instability may suggest a criterion for determining the formation number in a starting jet, which states that the leading vortex ring starts to pinch-off when the dimensionless parameter A of the starting jet decreases to a critical value $A_c \approx 1.1$. Moreover, since shear layer is actually an intrinsic component in many other vortex-shedding configurations, such as two-dimensional starting flow, vortex shedding in the wake of cylinder or vortex wake of an oscillating flat plate, one may speculate that the instability criterion for identify the onset of the pinch-off process can be applied to these vortex-shedding configurations. But the value of A_c would be subject to varying due to the different types of the flow.

6. Concluding remarks

Experiments using DPIV have been performed to investigate the effect of the trailing jet instability on the vortex ring pinch-off in starting jets. It is found that a series of secondary vortices start to develop only after the formation number is achieved. Subsequently, the growth of secondary vortices leads to the rapid decrease in the vorticity flux being fed into the leading vortex ring. When the vorticity flux vanishes, the leading vortex ring separates completely from the trailing jet, indicating the end of the pinch-off process. The roll-up and subsequent evolution of secondary vortices are found to depend on the induced radial velocity and the downstream translation of the leading vortex ring. According to the results of the linearized stability analysis for axisymmetric shear layer, the trailing shear layer is more unstable and has enough length to support the roll-up of secondary vortices after the formation number. A dimensionless parameter 'A', defined as $A = \Gamma_{ring}/x_{core}\Delta U$, has therefore been proposed to characterize limiting process of vortex ring formation in terms of the development of the trailing jet instability. Experimental results show that A decreases with the formation time. The perturbation that will later develop fully into the first secondary vortex is issued from the jet exit when a critical value $A_c = 1.1 \pm 0.1$ is reached, and it also corresponds to the onset of the pinch-off process.

From the experimental results and discussion in this paper, it is suggested that the formation and evolution of secondary vortices due to the trailing shear layer instability can be regarded as the underlying physical mechanism which constrains the growth of the leading vortex ring with larger circulation. The vortex ring pinch-off is actually the consequence of the decrease in vorticity flux being fed into the leading vortex ring due to the growth of secondary vortices.

Acknowledgements

Financial support from the Academic Research Grant Committee and studentships from the School of Mechanical and Aerospace Engineering for the first author are gratefully acknowledged.

REFERENCES

ADRIAN, R. J. & WESTERWEEL, J. 2010 *Particle Image Velocimetry*. Cambridge University Press.

ALLEN, J. J. & NAITOH, T. 2005 Experimental study of the production of vortex rings using a variable diameter orifice. *Phys. Fluids* **17**, 061701.

BENJAMIN, T. 1976 The alliance of practical and analytical insights into the nonlinear problems of fluid mechanics. *Appl. Methods Funct. Anal. Probl. Mech.* **503**, 8–29.

COHEN, J. & WYGNANSKI, I. 1987 The evolution of instabilities in the axisymmetric jet. Part 1. The linear growth of disturbances near the nozzle. *J. Fluid Mech.* **176**, 191–219.

DABIRI, J. O. & GHARIB, M. 2004 Delay of vortex ring pinchoff by an imposed bulk counterflow. *Phys. Fluids* **16**, L28.

DABIRI, J. O. & GHARIB, M. 2005 Starting flow through nozzles with temporally variable exit diameter. *J. Fluid Mech.* **538**, 111–136.

DIDDEN, N. 1979 On the formation of vortex rings: rolling-up and production of circulation. *J. Appl. Math. Phys. (Z. Angew. Math. Phys.)* **30** (1), 101–116.

DRING, R. P. 1982 Sizing criteria for laser anemometry particles. *Trans. ASME: J. Fluids Engng* **104** (1), 15–17.

GAO, L. & YU, S. C. M. 2010 A model for the pinch-off process of the leading vortex ring in a starting jet. *J. Fluid Mech.* **656**, 205–222.

GAO, L., YU, S. C. M., AI, J. J. & LAW, A. W. K. 2008 Circulation and energy of the leading vortex ring in a gravity-driven starting jet. *Phys. Fluids* **20**, 093604.

GHARIB, M., RAMBOD, E. & SHARIFF, K. 1998 A universal time scale for vortex ring formation. *J. Fluid Mech.* **360**, 121–140.

HJELMFELT, A. T. & MOCKROS, L. F. 1966 Motion of discrete particles in a turbulent fluid. *Appl. Sci. Res.* **16** (1), 149–161.

KELVIN, L. 1880 Vortex statics. *Phil. Mag.* **10**, 97–109.

KRUEGER, P. S., DABIRI, J. O. & GHARIB, M. 2006 The formation number of vortex rings formed in uniform background co-flow. *J. Fluid Mech.* **556**, 147–166.

KRUEGER, P. S. & GHARIB, M. 2003 The significance of vortex ring formation to the impulse and thrust of a starting jet. *Phys. Fluids* **15**, 1271.

LIM, T. T. 1997 A note on the leapfrogging between two coaxial vortex rings at low Reynolds numbers. *Phys. Fluids* **9**, 239.

MAXWORTHY, T. 1972 The structure and stability of vortex rings. *J. Fluid Mech.* **51** (01), 15–32.

MEI, R. 1996 Velocity fidelity of flow tracer particles. *Exp. Fluids* **22** (1), 1–13.

MICHALKE, A. 1971 Instability of a compressible circular free jet with consideration of the influence of the jet boundary layer thickness. *Z. Flugwissenschaften (West Germany)* **19** (8), 319–328.

MICHALKE, A. & HERMANN, G. 1982 On the inviscid instability of a circular jet with external flow. *J. Fluid Mech.* **114**, 343–359.

MOHSENI, K. & GHARIB, M. 1998 A model for universal time scale of vortex ring formation. *Phys. Fluids* **10**, 2436.

MOHSENI, K., RAN, H. & COLONIUS, T. 2001 Numerical experiments on vortex ring formation. *J. Fluid Mech.* **430**, 267–282.

MORRIS, P. J. 1976 The spatial viscous instability of axisymmetric jets. *J. Fluid Mech.* **77** (03), 511–529.

O'FARRELL, C. & DABIRI, J. O. 2010 A Lagrangian approach to identifying vortex pinch-off. *Chaos* **20**, 017513.

PAWLAK, G., MARUGAN CRUZ, C., MARTÍNEZ BAZÁN, C. & GARCÍA HRDY, P. 2007 Experimental characterization of starting jet dynamics. *Fluid Dyn. Res.* **39** (11–12), 711–730.

RILEY, N. & STEVENS, D. P. 1993 A note on leapfrogging vortex rings. *Fluid Dyn. Res.* **11** (5), 235–244.

ROSENFELD, M., RAMBOD, E. & GHARIB, M. 1998 Circulation and formation number of laminar vortex rings. *J. Fluid Mech.* **376**, 297–318.

SAFFMAN, P. G. 1965 The lift on a small sphere in a shear flow. *J. Fluid Mech.* **22**, 385–400.

SAFFMAN, P. G. 1968 Corrigendum to the lift on a small particle in a slow shear flow. *J. Fluid Mech.* **31**, 624.

SAFFMAN, P. G. 1995 *Vortex Dynamics*. Cambridge University Press.

SHUSSER, M. & GHARIB, M. 2000 Energy and velocity of a forming vortex ring. *Phys. Fluids* **12**, 618.

SHUSSER, M., GHARIB, M., ROSENFELD, M. & MOHSENI, K. 2002 On the effect of pipe boundary layer growth on the formation of a laminar vortex ring generated by a piston/cylinder arrangement. *Theor. Comput. Fluid Dyn.* **15** (5), 303–316.

TODDE, V., SPAZZINI, P. G. & SANDBERG, M. 2009 Experimental analysis of low-Reynolds number free jets. *Exp. Fluids* **47** (2), 279–294.

WILLERT, C. E. & GHARIB, M. 1991 Digital particle image velocimetry. *Exp. Fluids* **10** (4), 181–193.

ZHAO, W., FRANKEL, S. H. & MONGEAU, L. G. 2000 Effects of trailing jet instability on vortex ring formation. *Phys. Fluids* **12**, 589.